Proceedings of the 11th World Congress on Mechanical, Chemical, and Material Engineering (MCM'25)

Paris, France - August, 2025 Paper No. HTFF 124 DOI: 10.11159/htff25.124

# CFD Study on Cross-Cut Design of Horizontal Plate-Fin Heat Sinks

## Po-Hsun Chen, Chieh Yeh, Yu-Fu Ku

Thermal Analysis Design Center/Wistron NeWeb Corporation 20 Park Avenue II, Hsinchu Science Park Hsinchu 300, Taiwan Pohsun.Chen@wnc.com.tw; Jack.Yeh@wnc.com.tw; Ned.Ku@wnc.com.tw

**Abstract** - In this work, simulations are conducted to investigate the effect of the cross-cut design on reducing the so-called ineffective zone that has low velocity in a long horizontal plate-fin heat sink. The low-velocity region exists when the plate-fin channels are too long for air from one end to reach the centre, causing the reduction of thermal performance. It is found that the lateral flows penetrating into the low-velocity region through cuts on the fins prevents the heat sink from an incomplete usage and thus improves its thermal performance. In this numerical study, we found that the cut length ( $L_c$ ) and cut number ( $N_c$ ) are two crucial factors that affects the total heat transfer of a cross-cut heat sink. For the heat sink with length of 200 mm, height of 12 mm, width of 100 mm and spacing of 6.8 mm the best cut number along with the corresponding optimum cut length are  $N_c = 4$  and  $L_c = 12$  mm, with which the heat sink has improvement of 22.3% reduction in its temperature excess and 13.6% reduction in its weight.

**Keywords:** Plate-fin heat sink; Cross-cut design; Ineffective zone; Natural convection; Electronics cooling.

#### 1. Introduction

The plate-fin heat sink, where the finned surface expands convection areas and thus reduces the thermal resistance, is commonly used in electronics to improve the cooling. The fin number is often a topic of interest since excessive fins leads to an overly narrowed fin spacing that reduces the velocity of air moving along the fin channels. Bejan [1] derived the optimum fin spacing ( $s_{opt}$ ) of the vertical plate-fin heat sink that is able to achieve the maximum heat transfer with  $s_{opt} \sim 2.3 \text{Ra}_L^{-1/4} L$ , where L and L are the length of fin and Rayleigh number, respectively. The entropy generation minimization (EGM) is an alternative method commonly used in the optimization of designs [2]. Bhandari and Kulkarni [3] studied the optimum spacing using the algorithm of particle swarm optimization (PSO) to minimize the entropy generation, and Culham and Muzychka [4] extended the single parameter into multiple parameters including fin spacing and geometrical size of heat sink, the optimum values of which are solved uniquely by Newton-Raphson method. Khan et al. [5] then generalized Culham and Muzychka's method by Lagrange multipliers for application to solving constrained problems. These optimization algorithms utilized empirical equations in their objective functions whose minimization provided optimum design of plate-fin heat sink.

However, those empirical-based methods were seldom applied to optimum design for plate-fin heat sinks in horizontal placement because of its complex flow patterns in natural convection. Unlike a vertical heat sink from which only a single heat convection plume can be observed due to the same direction of channels and the buoyant force, a horizontal heat sink could arise either the single-plume or multiple-plume flows depending on its geometrical parameters [6]. The physical basis of the multiple-plume flow is that air entrance from the channel ends is not adequate to reach the channel centre before leaving the heat sink. As the multiple-plume flow emerges from a horizontal heat sink, the total heat transfer decreases since the portion of fin channels where air flow cannot reach has an extremely small heat transfer coefficient. This locally low heat transfer that reduces the average heat transfer causes inaccuracy in those conventional predictions that only consider the single-plume flow in their optimization algorithm.

The multiple-plume flow is experimentally and numerically observed in Harahap and McManus's experiment [6] and Wong and Huang's computational fluid dynamics (CFD) simulation [7][8], respectively. In Wong and Huang's numerical analysis they found the dynamic characteristics of the multiple-plume flow is a crucial factor in the estimation of convection heat transfer coefficients. Unsteady analysis yielded higher heat transfer coefficients than those evaluated by steady-state simulation. Although there were several studies on the correlations in term of heat transfer coefficient and geometrical parameters of plate-fin heat sink, Adhikari et al. [9] argued that the prediction of those correlations is limit in general and

often leads to contradictory results. In their study, Adhikari et al. proposed the optimization algorithm based on the results calculated using CFD and suggested that the design using the CFD-based optimization is more general than correlation-based optimization. Also, their method can be readily applied to other related studies, such as heat sinks with inclined fin array and the condition of combined forced and free convection.

In addition to optimizing the geometrical parameters, the thermal performance is also improved through the adjustment of fin arrangement or structure of horizontal heat sinks. Feng et al. [10] considered the cross-fin heat sink that two series of short fins are arranged perpendicularly to a series of middle long fins. In the study, the velocity and temperature fields indicated that the cold air entering those short fin channels is capable of traveling the entire channel and thus can minimize the areas with low h. Huang et al. [11] introduced the perforations in the base of heat sink for better ventilation. The middle portion of fins where the cold air originally hardly reach from the channel ends then can be cooled by the air entering from the bottom of base. In Tari and Ozet's study [12], they firstly found the longitudinal vortices in their study on the thermal performance related to inclination of a heat sink. These vortices imply the worse performance from the heat sink since they only exist in the region that the flow in the fin channels does not reach. To diminish such region, they proposed a couple of concepts including removing partial sections of fins to bring air into the low-velocity region, adding pin fins to generate disturbance that can break up the original flow structure, and enhancing the height of end fins to prevent the interference of lateral flows that prompt the separation of single plume. (See Ref. [13] for the detailed design.) The simulation results showed that only the approach using high end fins had remarkable effects on reduction of the low-velocity region.

Although the above methods provided improvement in the thermal performance on horizontal heat sinks, some designs might not be suitable for mass production from the aspect of manufacturing process, production cost or commercial consideration. For instance, for a limited package size requested by the customer, adjustment in the size of heat sinks using optimization algorithm may be not allowable for the designer. Also, perforation in the base of heat sink might not be practical when it comes to the application to electronic devices since heat sinks are often attached to ICs mounted on a printed circuit board (PCB) that blocks the path of flows below the heat sink. On the other hand, the plate-fin with special patterns (e.g., X-shaped cut) could enhanced the manufacturing cost due to the necessity of CNC machining. In this study, the improvement of horizontal heat sink will be achieved by a simple and realistic design: cross-cut heat sinks. This type of heat sinks has one or more transverse cuts perpendicular to the plate fins. (See [14][15] for more reference.) Although the cross-cut design is often used to interrupt the growth of boundary layers in the forced convection, it is rarely discussed on a horizontal heat sink in natural convection. Here, we will numerically study the effect of cross-cut designs on the thermal performance of heat sinks and conduct the parametric study in term of cut length ( $L_c$ ) and cut number ( $N_c$ ).

The remainder of this paper is organized as follows. Section 2 describes the computational model including the boundary conditions and geometry of tested heat sinks. In Section 3 the visualization of the flow paths and velocity distribution is followed by the discussion on the thermal performance of cross-cut heat sinks. In the end of paper, we summarize the remarkable findings and provides a simple guide for our cross-cut design in Section 4.

## 2. Methodology

In our numerical study, the simulations of three-dimensional, steady-state, incompressible, turbulent conjugate heat transfer is conducted using commercial CFD software, Simcenter Flotherm. The automatic algebraic turbulence model [16] is used in the computation. The governing equations with constant fluid and thermal properties are written as follows.

$$\rho \, \nabla \cdot \mathbf{U} = 0 \tag{1}$$

$$\rho(\mathbf{U} \cdot \nabla)\mathbf{U} = -\nabla p + \mu \nabla^2 \mathbf{U} + \rho \mathbf{g}$$
 (2)

$$\rho C_p(\mathbf{U} \cdot \nabla) T = k \nabla^2 T + S \tag{3}$$

Eq. (1) expresses the continuity of mass, where  $\rho$  and **U** are density and velocity of fluid. Eq. (2) is Navier-Stokes equations describing the motion of viscous fluid substance, where p,  $\mu$  and  $\mathbf{g}$  are the pressure, dynamic viscosity and gravitational

acceleration. Note that the magnitude of gravitational acceleration is set at  $|\mathbf{g}| = 9.81$  m/s<sup>2</sup>, and its direction determined by the placement of heat sinks is in the direction of  $-\mathbf{y}$  and  $-\mathbf{z}$  for the horizontal and vertical placements, respectively. The conservation of energy is given in Eq. (3), where T is temperature, k is thermal conductivity and  $C_p$  is specific heat capacity. The source term is denoted by S in the last term. The radiation exchange including the effect of direct and reflected radiation is modelled by the Surface-to-Surface (S2S) method with calculation of view factors between every two surfaces.

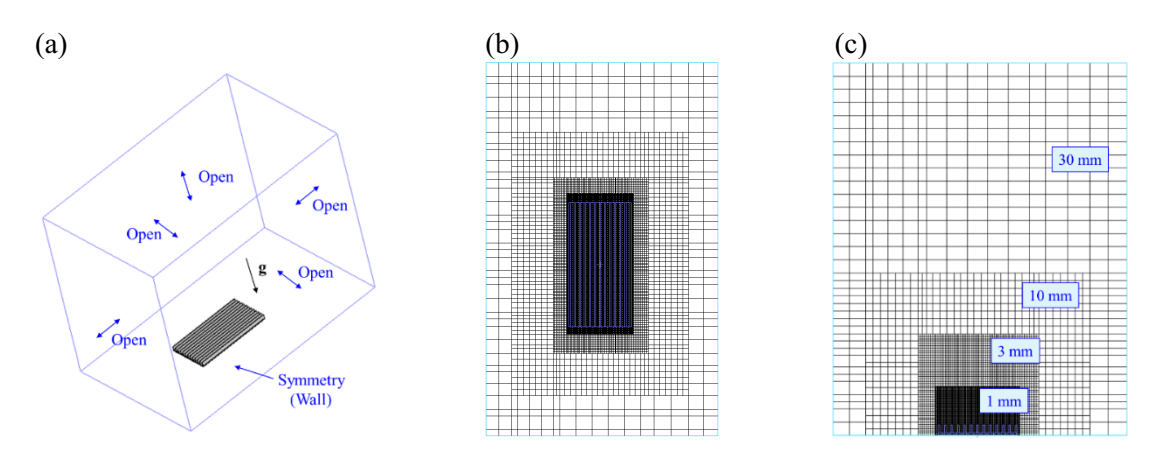


Fig. 1: (a) Computational domain, (b) computational grid in the top view and (c) grid in the front view.

Fig. 1(a) shows the computational domain with the five boundaries specified by "Open type" that have enough distance from the heat sink so that the influence of open boundaries on the flow near the heat sink can be neglected. The ambient temperature imposed on the open boundaries is set at  $T_a = 45^{\circ}$ C. The other boundary connected to the bottom of the heater is specified by "Symmetry type" that works as an adiabatic wall below the heater. The heat sink covering the heater has the same size of the base perfectly attached to the top of the heater. We chose two heat sinks with the length (L) of 100 and 200 mm, the width (W) of 100 mm, the height (H) of 12 mm including the fin (H) of 10 mm and the base (H) of 2 mm, and the fin thickness (H) of 2 mm. The heater has the same base area with the thickness (H) of 1 mm. The orthogonal mesh is used in the computational domain. Four-level grid sizes from the heat sink to the domain boundary are 1, 3, 10 and 30 mm as shown in Fig. 1(b) and (c). The minimum cell numbers between fins and within fins are constrained by 7 and 3 cells, respectively.

As a numerical study, the thermal properties in the system should be specified for computation. The air as the working fluid is specified constantly by  $\rho = 1.16 \text{ kg/m}^3$ ,  $\mu = 1.84 \times 10^{-5} \text{ Pa·s}$ , k = 0.0261 W/m·K and  $C_p = 1005 \text{ J/kg·K}$ . The heat sink and heater are made of Aluminum-6061 with k = 180 W/m·K and Copper with k = 385 W/m·K, respectively. Their radiation emissivities are both set as  $\varepsilon = 0.2$ . To heat up the heat sink, power inputs of 5 and 10 watts are uniformly distributed to the copper heater under the heat sink of L = 100 and 200 mm, respectively.

#### 3. Results and Discussions

#### 3.1. Vertical and Horizontal Uncut Heat Sinks

The two heat sinks of L = 100 and 200 mm have their theoretical optimum spacings in vertical placement, namely  $s_{\rm opt} = 6.6$  mm for L = 200 mm and  $s_{\rm opt} = 5.9$  mm for L = 100 mm, calculated by the formula  $s_{\rm opt} = 2.3 {\rm Ra_L}^{-1/4} L$  in Bejan's work [1]. At the start, let us have a glance at the flow patterns from the two heat sinks of different lengths with the same spacing of s = 6.2 mm that is close to the theoretical values mentioned above. Fig. 2 presents the pathlines from the vertical heat sinks of (a) L = 100 mm, (b) L = 200 mm, the horizontal heat sinks of (c) L = 100 mm and (d) L = 200 mm. The pathlines in Fig. 2(a) and (b) show the same flow pattern from the vertical heat sinks regardless of the length of heat sinks, while in Fig. 2(c) and (d) a single plume from the shorter horizontal heat sink separates into multiple plumes as L becomes longer. The location where longitudinal flows turn into upward plumes depends on the result of competition between the longitudinal momentum that drives flow forward to the channel centre and the buoyant force in the opposite direction of gravitational acceleration

that attempts to take flow out of channel. That is, in a long channel the longitudinal flows are readily taken upward by the buoyance before reaching the channel centre. Note also that the vortices driven by lateral flows emerge in the section of channel that the longitudinal flow does not reach.

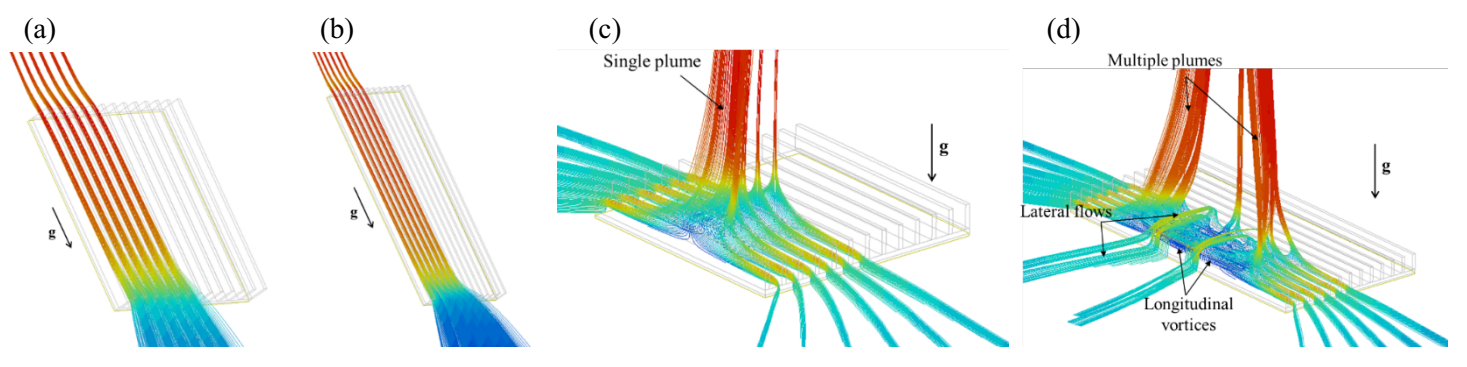


Fig. 2: Pathlines within uncut plate fins in (a) vertical heat sink of L = 100 mm, (b) vertical one of L = 200 mm, (c) horizontal one of L = 100 mm and (d) horizontal one of L = 200 mm, with spacing of s = 6.2 mm. Pathlines are only presented at the first six channels and the symmetrical ones at the rest of six channels are omitted for clarity.

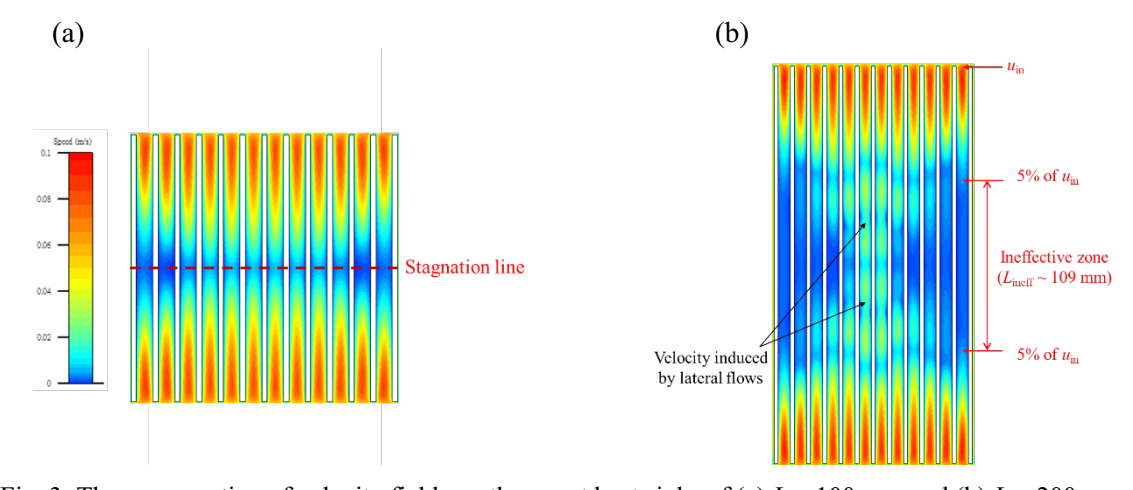
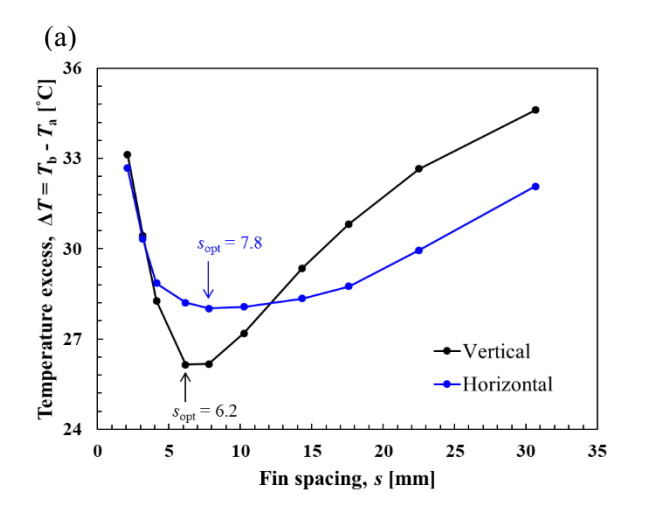


Fig. 3: The cross section of velocity fields on the uncut heat sinks of (a) L = 100 mm and (b) L = 200 mm.

For more clarity, the velocity fields within channels at h/2 are presented in Fig. 3. In Fig. 3(a) the cold air passes the short channels thoroughly, and the stagnation line occurs at the centre due to collision of flows coming from opposite channel ends. On the other hand, in Fig. 3(b) the low velocity region indicates the section of channels where flows cannot reach, although some velocity induced by lateral flows exists in the middle channels. We referred to such region with low speed as *ineffective zone*, the region with extremely low heat transfer. The ineffective zone is the very factor that crucially compromises the thermal performance of a horizontal heat sink. As described in Fig. 3 (b), here we only considered the first fin channel and defined the boundary of the ineffective zone at the location where only 5% of inlet velocity remains. Taking the heat sink we used in Fig. 3 (b) (i.e., L = 200 mm and s = 6.2 mm) for instance, the length of ineffective zone denoted by  $L_{\text{ineff}}$  is estimated to be 109 mm. Table 1 lists  $L_{\text{ineff}}$  and  $\Delta T_{\text{uncut}}$  (defined by  $T_b - T_a$ , where  $T_b$  is the base centre temperature) at all distinct spacings for uncut heat sinks. It is noticed that the ineffective zone expands as the heat sink with  $s \le 7.8$  mm has a narrower spacing because of a smaller inlet area (i.e., hs) of cold air, while there is the single-plume flow and thus no ineffective zone for the one with  $s \ge 10.3$  mm.

Although Tari and Mehrtash's study [12] implies that the choice of the vertical or horizontal placement of a heat sink might have minor influence on its thermal performance and optimum spacings, this conclusion only held true for the absence of ineffective zone. Fig. 4 depicts  $\Delta T$ , the temperature excess, at different fin spacings for both vertical and horizontal heat sinks of L = 100 and 200 mm. Since the multiple-plume flow and ineffective zone is absent in the heat sink of L = 100 mm with s = 6.2 mm referred to Fig. 2(a) and (c), it agrees with Tari and Mehrtash's results that  $s_{\text{opt}} = 7.8$  mm for horizontal placement is close to  $s_{\text{opt}} = 6.2$  mm for vertical placement as shown in Fig. 4(a). Conversely, emergence of the ineffective zone not only reduces the thermal performance but also suggests the necessity of a larger spacing to allow more air flow in each channel. As a result, the horizontal uncut heat sink of L = 200 mm has much wider optimum spacing of  $s_{\text{opt}} = 17.6$  mm than the  $s_{\text{opt}} = 7.8$  mm for the heat sink in vertical placement as shown in Fig. 4(b). Yet, we think that 17.6 mm is not its actual optimum spacing. To improve thermal performance, we can narrow down the ineffective zone as well as optimum spacing (for a denser fin number) through the cross-cut design discussed in the next section.



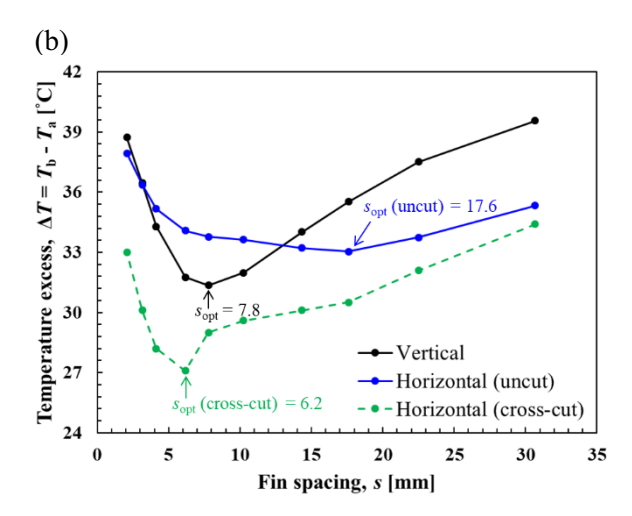


Fig. 4: Variation of temperature excesses at the bottom center on the uncut heat sinks of (a) L = 100 mm and (b) L = 200 mm, with a varied spacing from 2.1 to 30.7 mm. The extremes are indicated by  $s_{\text{opt}}$  for both vertical and horizontal heat sinks.

s [mm]	30.7	22.5	17.6	14.3	10.3	7.8	6.2	4.1	3.2	2.1
$\Delta T_{\mathrm{uncut}}  [^{\circ}\mathrm{C}]$	35.3	33.7	33.0	33.2	33.6	33.8	34.1	35.2	36.4	37.9
Type of plume	Single	Single	Single	Single	Single	Multiple	Multiple	Multiple	Multiple	Multiple
$L_{ineff}\left[mm ight]$	0	0	0	0	0	42	109	124	136	149
$N_{ m c}$	1	1	1	1	1	2	2	2	2	2
$\Delta T_{ m cut}  [^{\circ}{ m C}]$	34.4	32.1	30.5	30.1	29.6	29.0	27.1	28.2	30.1	33.0
L <sub>c</sub> [mm]	18	18	12	12	15	12	18	21	21	21

Table 1: The temperature excesses of the uncut and cross-cut horizontal heat sinks of L = 200 mm with varied spacings.

## 3.2. Cross-Cut Design for Smaller $s_{opt}$

In Fig. 3(b) the velocity field depicts the ineffective zone where air leaves the heat sink prematurely before reaching the channel centre. To address the deficit of the air entrance, in our idea the ineffective zone can be removed by introducing cold air from the lateral flow through the cuts. To verify this idea, for the multiple-plume cases listed in Table 1 (i.e.,  $s \le 7.8$  mm), we add two cuts on each heat sink at the locations symmetrical to the channel centre. The two cuts and the central line "equally" divide  $L_{\text{ineff}}$  with the cut length of  $L_{\text{c}} = 3$ , 6, 9, ..., 27 mm. For heat sinks with  $s \ge 10.3$  mm that have no ineffective zone as discussed in Sect.3.1, we also add one cut at the channel centre to observe their change of thermal performance.

For each s, the lowest temperature excesses denoted by  $\Delta T_{\rm cut}$  are shown in Fig. 4(b), while the corresponding  $L_{\rm c}$  can be found in the last row of Table 1. For all fin spacings chosen in the simulation, the cross-cut heat sinks have lower  $\Delta T$  and thus lower thermal resistances than the uncut heat sink with the same spacing. In the case of  $s \le 7.8$  mm, the lateral flow invades into the ineffective zone through the gaps of intercepted fins, which facilitates an effective usage of the entire heat sink. With the ineffective zone being removed by the lateral flow from the gaps, the optimum spacing of the heat sink then can be narrowed down from 17.6 mm to 6.2 mm as shown in Fig. 4(b), which is close to the optimum spacing in vertical placement. Under the condition of having no ineffective zone, the heat sink with denser fins s = 6.2 mm provides a larger heat transfer area and hence the better thermal performance than the heat sink with s = 17.6 mm. The temperature excess of 33.0°C in the originally optimum uncut heat sink with s = 17.6 mm, specifically, is reduced into 27.1°C in the 2-cut heat sink with s = 6.2 mm and s = 18 mm. There is an improvement of 18% using the cross-cut design on the horizontal heat sink of s = 18 mm. There is an improvement of 18% using the cross-cut design on the horizontal heat sink of s = 18 mm.

On the other hand, the 1-cut heat sinks with  $s \ge 10.3$  mm also provide better thermal performances than the original uncut heat sinks though there is no ineffective zone in the original ones. As we have known, the flow in fin channels is always companied by the resistance and heating from fins and it gets slower and warmer on its journey. As a result, the flow at the channel centre has lowest speeds along with warmest air, which leads to the continuous reduction of heat transfer effectiveness along the path of air flow in the channel. By adding one cut at the centre, the channel centre is replenished with the cold air laterally from the channel sides. For both the 1-cut and the 2-cut heat sinks, larger  $L_c$  introduces more cold air into fin channels, but at the same time the heat transfer area decreases. Hence, for a given spacing an optimum  $L_c$  could be found to achieve the best thermal performance as listed in the last row of Table 1.

## 3.3. Cut Number of the Cross-Cut Designs

While the previous sections have covered the effect of having cuts instead of none, the cut number ( $N_c$ ) was not discussed. In this section, we would further discuss the effect of different  $N_c$  on the thermal performance. Here we choose five different cut numbers, namely  $N_c = 1, 2, 4, 6, 8$ , and apply to the same heat sink of L = 200 mm with s = 6.2 mm. As discussed in Sect. 3.2, except for the 1-cut design that has one cut on the central line of fin channels, the others with  $N_c > 1$  are cut at the symmetric locations where the cuts and the central line equally divide  $L_{ineff}$  of uncut heat sinks. [Referred to Table 1,  $L_{ineff}$  is 109 mm in the heat sinks of L = 200 mm with s = 6.2 mm.] Note that all cuts on a heat sink are set at the same  $L_c$  in our design. Fig. 5 presents the cross section of velocity fields in the five different  $N_c$  with  $L_{c,tot} = 48$  mm, where  $L_{c,tot}$  is the total length of the cuts (i.e.,  $L_{c,tot} = N_c \times L_c$ ). The location of the cuts, which divide  $L_{ineff}$  evenly, are chosen because the flow invading from the cuts is observed to penetrate the same distance in both directions in the channel. Thus, putting the cuts at the chosen location is a simple and straightforward way to make invading lateral flows evenly distribute in the ineffective zone.

For a given power of 10 watts, the temperature excesses of the cross-cut heat sink are depicted in Fig. 6. While the same  $L_{c,tot}$  in heat sinks with different  $N_c$  would imply the same open ratio for introducing the lateral air flow and the same reduction in their weight, the optimum  $L_{c,tot}$  is found to be varying with different  $N_c$ . The lowest  $\Delta T$  in 1-cut, 2-cut, 4-cut, 6-cut and 8-cut heat sinks (i.e.,  $L_{c,tot} = 18, 36, 48, 60, 72$  mm) are 29.7, 27.1, 26.5, 27.4 and 28.6°C with the corresponding optimum total cut lengths, respectively. For all cross-cut designs compared to the uncut one, the 4-cut heat sink has the most temperature reduction at  $L_{c,tot} = 48$  mm, namely 7.6°C, and it reduces 33.7 g (i.e., 13.6%) from the uncut heat sink of 248.4 g. It is no surprise that there is an optimum number for  $N_c$ , as shown in Fig. 6. For a very small cut number (e.g.,  $N_c = 1$ ) the lateral invading flows cannot be evenly distributed in the ineffective zone, while with an over large number (e.g.,  $N_c = 8$ ) the heat sink would have a large number of stagnation lines that decreases average velocity of the invading lateral flows. It should be noted that in this case, even with sub-optimum  $N_c$  and  $L_{c,tot}$ , all the cross-cut heat sinks still perform better than the uncut heat sink.

(a)	(b)	(c)	(d)	(e)
()	(-)	(-)	()	(-)

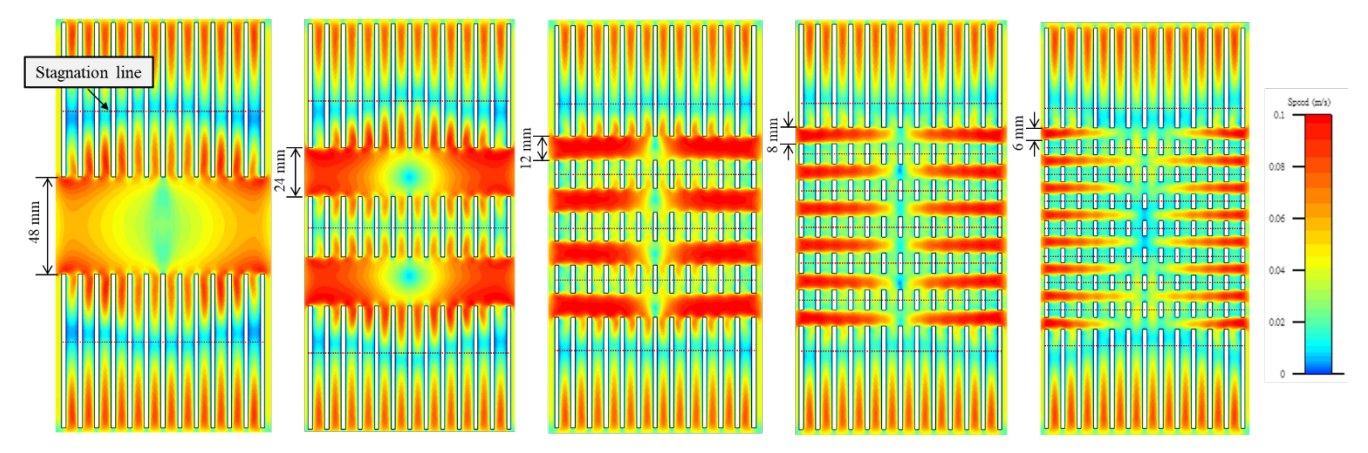


Fig. 5: Velocity fields on the 1-cut, 2-cut, 4-cut, 6-cut and 8-cut heat sinks with  $L_{c,tot} = 48$  mm and s = 6.2 mm. The dotted lines indicate stagnation lines where the opposite longitudinal flows collide.

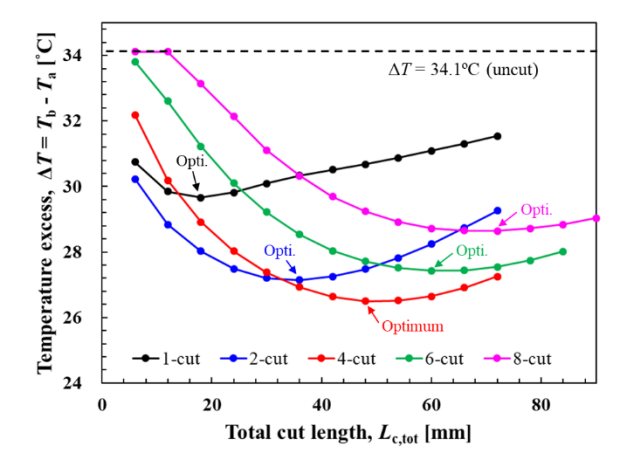


Fig. 6: Variation of temperature excesses with varied  $L_{c,tot}$  and the fixed spacing at s = 6.2 mm. The optimum  $L_{c,tot}$  with which heat sink has the lowest  $\Delta T$  is indicated for each cross-cut design. The dashed line notes  $\Delta T = 34.1$ °C from the uncut heat sink.

#### 4. Conclusion

In the study, the ineffective zone in the horizontal plate-fin heat sinks has been visualized using steady-state numerical simulation. The incomplete usage of the heat sink due to the ineffective zone gives designer an unreal and overlarge optimum spacing that leads to underestimation for the total heat transfer. Through the simple and widely-used cross-cut design, the cold air from lateral flows is introduced into the ineffective zone to achieve complete usage of the heat sink. In the present example of heatsink with L = 200 mm, the optimum spacing originally at 17.6 mm of the uncut heat sink is narrowed down to 6.2 mm after adoption of the 2-cut design with  $L_c = 18$  mm, which turns out 18% reduction in  $\Delta T$ . Even there is no ineffective zone for the case of  $s \ge 10.3$  mm, the cross-cut design with  $N_c = 1$  can also improve the thermal performance by replacing the warmer air at the channel centre with the cold air from lateral flows. In the study,  $L_c$  and  $N_c$  are found to be the two crucial factors that affects the thermal performance of a cross-cut heat sink. Overly small  $L_c$  is incapable of providing adequate cold air from lateral flows, whereas overly large  $L_c$  would reduce much of heat transfer area. Also, overly small  $N_{\rm cut}$  makes an uneven distribution of the penetrating air from lateral flows, while overly large  $N_c$  increases too many stagnation lines that reduces average flow speed within channels. Consequently, both of parameters have their optimum

values to achieve the maximum total heat transfer. In the case of L = 200 mm, we obtained the best  $N_c$  along with the corresponding optimum  $L_c$ , namely  $N_c = 4$  and  $L_c = 12$  mm, by conducting the numerical experiment. The heat sink got the improvement of 22.3% reduction of the temperature excess and 13.6% reduction of the heat sink weight. The correlation of geometrical parameters and the best  $N_c$  with optimum  $L_c$  will be the next study in the near future.

# Acknowledgements

The authors would like to thank the colleagues in thermal analysis design center for their comments on this study. The research is financially supported by Wistron NeWeb Coporation (WNC).

#### References

- [1] A. Bejan, Convection Heat Transfer. John wiley & sons, 2013.
- [2] A. Sciacovelli, V. Verda and E. Sciubba, "Entropy generation analysis as a design tool A review," *Renew. Sustain. Energy Rev.*, vol. 43, pp. 1167-1181, 2015.
- [3] V. S. Bhandari and S. H. Kulkarni, "Optimization of heat sink for thyristor using particle swarm optimization," *Res. Eng.*, vol. 4, 100034, 2019.
- [4] J. R. Culham and Y. S. Muzychka, "Optimization of plate fin heat sinks using entropy generation minimization," *IEEE Trans. Compon. Packag. Technol.*, vol. 24, no. 2, pp. 159-165, 2001.
- [5] W. A. Khan, J. R. Culham, and M. M. Yovanovich, "Optimization of pin-fin heat sinks using entropy generation minimization," *IEEE Trans. Compon. Packag. Technol.*, vol. 28, no. 2, pp. 247-254, 2005.
- [6] F. Harahap and H. N. McManus, Jr., "natural convection heat transfer from horizontal rectangular fin arrays," *J. Heat Tran.*, vol. 89, no. 1, pp. 32-38, 1967.
- [7] G. J. Huang and S. C. Wong, "Dynamic characteristics of natural convection from horizontal rectangular fin arrays," *Appl. Therm. Eng.*, vol. 42, pp. 81-89, 2012.
- [8] S. C. Wong and G. J. Huang, "Parametric study on the dynamic behavior of natural convection from horizontal rectangular fin arrays," *Int. J. Heat Mass Transf.*, vol. 60, pp. 334-342, 2013.
- [9] R. C. Adhikari, D. H. Wood and M. Pahlevani, "Optimizing rectangular fins for natural convection cooling using CFD," *Therm. Sci. Eng. Prog.*, vol. 17, 100484, 2020.
- [10] S. Feng, M. Shi, H. Yan, S. Sun, F. Li, and T. J. Lu, "Natural convection in a cross-fin heat sink," *Appl. Therm. Eng.*, vol. 132, pp. 30-37, 2018.
- [11] G. J. Huang, S. C. Wong and C. P. Lin, "Enhancement of natural convection heat transfer from horizontal rectangular fin arrays with perforations in fin base," *Int. J. Therm. Sci.*, vol. 84, pp. 164-174, 2014.
- [12] I. Tari and M. Mehrtash, "Natural convection heat transfer from horizontal and slightly inclined plate-fin heat sinks," *Appl. Therm. Eng.*, 61(2), 728-736, 2013.
- [13] I. Tari and M. E. Ozet, "Numerical investigation of various approaches to avoid natural convection instabilities inside the channels of horizontal plate fin heat sinks," in *Proceedings of the ASME 2016 IMECE*, Arizona, USA, 2016, vol. 8, V008T10A035.
- [14] T. Y. Kim and S. J. Kim, "Fluid flow and heat transfer characteristics of cross-cut heat sinks," *Int. J. Heat Mass Transf.*, vol. 52, no. 23-24, pp. 5358-5370, 2009.
- [15] S. Chingulpitak, N. Chimres, K. Nilpueng and S. Wongwises, "Experimental and numerical investigations of heat transfer and flow characteristics of cross-cut heat sinks," *Int. J. Heat Mass Transf.*, vol. 102, pp. 142-153, 2016.
- [16] D. Agonafer, L. Gan-Li and D. B. Spalding, "The LVEL turbulence model for conjugate heat transfer at low Reynolds numbers," in *Proceedings of the ASME 1996 IMECE*, Georgia, USA, 1996, vol. 18, pp. 23-26.